Massachusetts Institute of Technology

The peptide hormone glucagon forms amyloid fibrils with two coexisting β-strand conformations

Martin D. Gelenter[1], **Katelyn J. Smith**[2,$], **Shu-Yu Liao**[1,$], **Venkata S. Mandala**[1], **Aurelio J. Dregni**[1], **Matthew S. Lamm**[2], **Yu Tian**[3], **Wei Xu**[2], **Darrin J. Pochan**[3], **Thomas J. Tucker**[4], **Yongchao Su**[2,*], and **Mei Hong**[1,*]

[1]Department of Chemistry, Massachusetts Institute of Technology, Cambridge, Massachusetts, USA

[2]Pharmaceutical Sciences, Merck & Co., Inc., Kenilworth, New Jersey, USA

[3]Department of Materials Science and Engineering, University of Delaware, Newark, Delaware, USA

[4]Discovery Chemistry, Merck & Co., Inc., Kenilworth, New Jersey, USA

Abstract

Glucagon and insulin maintain blood glucose homeostasis and are used to treat hypoglycemia and hyperglycemia in diabetic patients, respectively. Whereas insulin is stable for weeks in its solution formulation, glucagon fibrillizes rapidly at the acidic pH required for solubility, and is therefore formulated as a lyophilized powder that is reconstituted in acidic solution immediately before use. Here we use solid-state NMR to determine the atomic-resolution structure of fibrils of synthetic human glucagon grown at pharmaceutically relevant low pH. Unexpectedly, two sets of chemical shifts are observed, indicating the coexistence of two β-strand conformations. Those two conformations have distinct water accessibilities and intermolecular contacts, indicating that they alternate and hydrogen-bond in an antiparallel fashion along the fibril axis. Two antiparallel β-

sheets assemble with symmetric homodimer cross sections. This amyloid structure is stabilized by numerous aromatic, cation-π, polar and hydrophobic interactions, suggesting mutagenesis approaches to inhibit fibrillization to improve this important drug.

Many peptides and proteins have a propensity to misfold and aggregate into amyloid fibrils, which consist of extended cross-β sheets with hydrogen bonds along the fibril axis[1]. For pharmaceutical peptides, this aggregation propensity presents a major challenge in drug formulation[2], because the efficacy of peptide drugs requires both high bioavailability and physical stability. Glucagon and insulin are peptide hormones responsible for blood sugar homeostasis, and are used in the management of blood sugar levels in diabetic patients. Insulin lowers the blood glucose level by increasing tissue uptake of glucose, and in its standard solution formulations is stable at room temperature for many weeks[3]. In contrast, glucagon raises the blood glucose level and treats severe hypoglycemia[4]. However, at the pharmaceutical concentration of ~1 mg/ml, glucagon is insoluble at neutral pH, and becomes soluble at basic pH (greater than 9) but undergoes chemical degradation[5]. At an acidic pH of less than 3, glucagon is both soluble and chemically stable, but fibrillizes within hours[6]. Therefore, the most common FDA-approved formulation of glucagon consists of a lyophilized peptide hydrochloride powder that is reconstituted into acidic solution immediately prior to administration. Elucidating the molecular structure of low-pH glucagon fibrils is thus crucial for achieving stable solution-state formulations of glucagon to enable the implementation of dual insulin/glucagon pumps as an "artificial pancreas" for diabetic patients.

X-ray diffraction (XRD), Fourier-transform infrared spectroscopy (FT-IR), transmission electron microscopy (TEM), and atomic force microscopy (AFM) have been used to characterize the hydrogen bonding, widths and morphologies of glucagon fibrils prepared under a variety of conditions[7–12]. However, these studies gave inconclusive results and no atomic-level structural information on any of the fibril polymorphs. Most known amyloid fibril structures formed by proteins that are implicated in neurodegenerative diseases show parallel-in-register cross-β sheets, which often coexist with dynamically disordered domains[13–16]. Only microcrystals of short peptide fragments have been observed to be able to form thermodynamically stable, antiparallel and fully rigid structures[17]. This observation has led to the hypothesis that the parallel-in-register cross-β motif may be the thermodynamically favored structure for all full-length amyloid fibrils, because it maximizes favorable hydrophobic interactions as well as polar interactions along the fibril axis[18]. In addition to the predominance of parallel-in-register β-sheet structures, solid-state NMR and TEM data of Alzheimer's Aβ peptides and other neurodegenerative amyloid fibrils have shown that each ultrastructural fibril morphology corresponds to a single molecular conformation with a single mode of intermolecular assembly[19–21].

We have now determined the atomic structure of glucagon fibrils formed under pharmaceutically relevant concentration and pH. Using solid-state nuclear magnetic resonance (NMR) spectroscopy and ^{13}C, ^{15}N-labeled peptides, we measured conformation-dependent ^{13}C and ^{15}N chemical shifts of the full-length peptide and numerous intramolecular and intermolecular distance restraints, thus determining the three-

dimensional structure and intermolecular packing of the glucagon fibrils. Strikingly, glucagon fibrillizes into a pair of antiparallel β-sheets that harbor two distinct molecular conformations alternating along the fibril axis. This structural motif has not been observed in any other amyloid fibrils to date, and demonstrates a unique case of molecular structural polymorphism within a single ultrastructural morphology. Moreover, this structure suggests future strategies for developing glucagon analogs that resist fibril formation.

Results

Glucagon forms homogeneous fibrils with two distinct conformers

We produced glucagon fibrils from 8 mg/mL solutions at pH 2 under quiescent conditions. Two types of ^{13}C, ^{15}N-labeled peptides were synthesized (Table 1): samples containing scattered labeled residues allow the measurement of well-resolved spectra with unambiguous long-range inter-residue distance restraints, whereas samples with consecutively labeled residues allow sequence-specific resonance assignment. Fibrils formed at ambient temperature over the course of 7 days with highly reproducible morphology and kinetics. Within 12 hours, the aggregates already took on a predominantly β-strand conformation, as evidenced by circular dichroism (CD) spectra (Fig. 1a). Dynamic light scattering (DLS) data show a progressive increase of the average particle size and polydispersity of particle sizes over a week (Fig. 1b). At the end of 7 days, mature fibrils measure ~1 μm in length, 6–10 nm in widths (Fig. 1c), and are predominantly straight[7].

Consistent with the homogeneous fibril morphology, magic-angle-spinning (MAS) solid-state NMR spectra of the fibrils show narrow ^{13}C linewidths of 0.6–0.9 ppm and ^{15}N linewidths of 1.0–1.3 ppm (Supplementary Figs. 1–3), indicating structural homogeneity at the molecular level. Unexpectedly, two sets of equal-intensity peaks are observed for the entire peptide (Fig. 2a–c), indicating the coexistence of two distinct molecular conformations at a 1 : 1 ratio. The average chemical shift difference per residue exceeds 0.5 ppm from Q3 to Y13 and from F22 to T29 while being smaller for the central residues (Fig. 2e).

Glucagon forms a rigid β-strand spanning a length of ~10 nm

Two- and three-dimensional (2D and 3D) ^{15}N-^{13}C correlation spectra (Fig. 2b,d and Supplementary Fig. 4) allowed the assignment of all ^{13}C and ^{15}N chemical shifts to the amino acid residues in the peptide and distinguished the two conformers on the basis of sequential cross peaks and long-range correlations between residues that are well separated in the amino acid sequence. Most Cα and CO chemical shifts are smaller than random coil values whereas the Cβ chemical shifts are larger than random coil values (Supplementary Fig. 5 and Supplementary Table 1), indicating uniform β-strand (φ, ψ) torsion angles for both conformers (Fig. 2f, Supplementary Table 2). The lack of (φ, ψ) angle variations is surprising, because most β-strands in known amyloid fibril structures and in β-barrel membrane proteins contain fewer than 10 residues, spanning ~3 nm[20,22], whereas a straight β-strand formed by a 29-residue peptide would span an extraordinary length of ~10 nm.

Glucagon assembles into antiparallel hydrogen-bonded β-sheets

To verify whether glucagon indeed forms a continuous β-strand, and to determine how multiple peptide chains associate with each other in the fibril, we measured long-range 2D ^{13}C-^{13}C correlation spectra. Using ^{13}C spin diffusion (SD) with 250 ms and 500 ms mixing, proton-assisted recoupling (PAR)[23] with 12 ms mixing, and Proton-Enhanced Rotor-echo Short Pulse IRradiATION Cross-Polarization (^{PERSPIRATION}CP)[24] with 15 ms mixing, we detected many correlation peaks between residues at the two ends of the peptide, such as S8–V23, T5–M27 and H1–T29 (Fig. 3a–c, Supplementary Fig. 6a–d). To distinguish whether these long-range correlations result from intramolecular contacts due to a strand-turn-strand fold[20], or intermolecular contacts due to antiparallel packing of multiple β-strands, we mixed labeled peptide with unlabeled peptide in a 1 : 3 ratio before fibrillization and measured their spectra. All long-range cross peak intensities decreased by approximately the dilution factor of 4 (Fig. 3a, Supplementary Fig. 7), proving that these long-range correlations are intermolecular in origin. Moreover, for each pair of correlated residues, only two, not four, cross peaks are observed, indicating that the correlation is exclusively intermolecular, between conformer I and conformer II, and not a combination of intermolecular (I-II) and intramolecular (I-I and II-II), thus ruling out a strand-turn-strand fold. The sum of the residue numbers for these long-range correlations ranges from 30 to 32 (Fig. 3e), indicating that multiple chains associate with each other with a well-defined antiparallel registry.

So far, all known high-resolution structures of naturally occurring amyloid fibrils have parallel-in-register hydrogen bonds along the fibril axis[13–15,20,25], with the exception of the D23N mutant of Aβ$_{1–40}$, which forms either a thermodynamically favored parallel-in-register cross-β fibril or a kinetically favored antiparallel cross-β fibril[26]. The surprising antiparallel arrangement of glucagon β-strands could in principle occur either via backbone N-H···O=C hydrogen bonds or via sidechain packing. To determine which scenario is correct, we measured ^{13}C-detected ^1H-^1H spin diffusion (CHHC) spectra[27]. For hydrogen-bonded antiparallel β-sheets, intermolecular Hα-Hα distances are much shorter than their intramolecular counterparts, thus strong Cα-Cα cross peaks are expected for antiparrel hydrogen-bonded β-sheets but not for parallel β-sheets. Using a short ^1H spin diffusion time of 200 μs, we observed many strong Cα-Cα cross peaks such as S8–V23 and T5–L26 in the CHHC spectra (Fig. 3d, Supplementary Figs. 6e, f), indicating that glucagon assembles into antiparallel hydrogen-bonded β-sheets.

The two conformers have different water-exposed surfaces

What is the origin of the dual molecular conformations when the fibril morphology is homogeneous? To answer this question, we measured water-edited 2D ^{13}C-^{13}C correlation spectra (Fig. 3f, Supplementary Fig. 8) to detect well-hydrated residues[28,29]. Water ^1H polarization can transfer to proteins through chemical exchange[30,31] and ^1H spin diffusion[32]. Both mechanisms lead to higher intensities for the water-exposed residues compared to residues sequestered in a dry interior. In a well-ordered β-sheet, the sidechains of two sequential residues point in opposite directions, thus odd-numbered sidechains should face one side of the β-sheet plane while even-numbered sidechains should face the other side. Interestingly, the water-transferred cross peak intensities of odd-numbered residues such as

T5, T7 and A19 are significantly higher in conformer II than in conformer I, while the water-transferred intensities of even-numbered residues such as S8 and V28 are higher in conformer I than in conformer II. Therefore, conformer I and conformer II have different wet and dry interfaces: conformer I packs odd-numbered residues at the dry steric-zipper interface whereas conformer II uses even-numbered residues to form the steric zipper.

Both conformers form homodimers in the fibril cross section

We further compared the cross peak intensities of diluted and undiluted peptides (Supplementary Fig. 7). Dilution decreased the intensities of intra-residue cross peaks such as T5$^{I/II}$ Cβ-Cγ_2 and Cβ-Cα relative to the diagonal Cβ peak by about 50%, indicating that some of the cross peak intensities result from intermolecular contact between T5 sidechains in two monomers. Sequential cross peaks such as T5$^{I/II}$ Cβ – F6$^{I/II}$ Cα also decreased by ~50%, indicating that these sequential cross peaks also contain both intramolecular and intermolecular contributions. Furthermore, some of the long-range correlations manifest only one of the two I-II combinations, indicating asymmetry between the two conformers. For example, multiple T5^{II}-M27^{I} cross peaks are observed but no corresponding T5^{I}-M27^{II} cross peaks are detected (Fig. 3a), indicating that the M27 sidechain is in close proximity to T5 and other residues in conformer I but extends into water in conformer II. Finally, the two V23 Cγ chemical shifts are split by 1.4 ppm in conformer I but are averaged to a single peak in conformer II (Fig. 2a, Supplementary Fig. 7a), indicating that the V23 sidechain is stabilized in conformer I by hydrophobic interactions with V23 across the homodimer interface, but is water-exposed and undergoes torsional fluctuations in conformer II.

These water accessibility, dilution and asymmetric sidechain structural data together indicate that the two β-strand conformations in the glucagon fibril are distinguished by interdigitation of alternate sidechains at the steric-zipper interfaces (Fig. 3h, Supplementary Fig. 9a)[17]. In conformer I odd-numbered sidechains, such as Y13 and W25 form the steric zipper whereas in conformer II even-numbered sidechains, such as F6, Y10 and L26 form the dry interface. Within each cross section normal to the fibril axis, the β-strands align in parallel with C$_2$ symmetry about an axis parallel to both peptide backbones. The basic structural unit of the low-pH glucagon fibril is therefore a dimer-of-dimers that contains antiparallel backbone hydrogen-bonding and parallel steric zippers with symmetry-breaking sidechain conformations in alternating layers. In addition to favorable I-I and II-II homomeric interactions, there are favorable sidechain interactions in the heteromeric interface, further stabilizing the assembly (*vide infra*). This β-sheet assembly corresponds to the class-8 steric zipper that has been observed in microcrystals of small peptides[17].

Glucagon fibril structure reveals stabilizing interactions

We calculated the structure of the low-pH glucagon fibrils using 350 intramolecular correlations (Supplementary Fig. 9d), 285 intermolecular correlations (Supplementary Fig. 9e), and 54 (φ, ψ) torsion angles predicted from chemical shifts. The resulting lowest-energy structural ensemble (Fig. 4a, b) shows a pairwise backbone root-mean-square deviation (RMSD) of 0.80 Å and a pairwise heavy-atom RMSD of 1.67 Å (Table 2).

The structure shows many favorable sidechain interactions such as a tetrameric "aromatic box" at F6–W25, polar interactions at Q3–N28, T7–Q24, S11–Q20 and D15-S16, cation-π interactions at Y13-R18, and steric complementarity at M27-G4 (Fig. 4c, d). Although the two R18[II] sidechains at the homodimer interface are expected to cause unfavorable electrostatic repulsion, this interaction is mitigated by the favorable heteromeric Y13[I]-R18[II] cation-π interaction. It is known that cation-π interactions contribute 0.5–2.5 kcal/mol to protein stability[33], whereas aromatic π-stacking interactions provide 0.5–1.5 kcal/mol of stabilization[34,35]. Polar interactions such as those involving Asn sidechains in hydrophobic environments contribute 0.5–2.0 kcal/mol of stability[36,37], whereas each hydrogen bond in β-sheet backbones contributes 1–2 kcal/mol of stability[38]. These interactions thus provide considerable stability to the dimer-of-dimer β-sheet structure of the glucagon fibril. The homodimer in the fibril cross section has a thickness of ~2 nm, consistent with the average height of 1.97 ± 0.22 nm obtained from atomic force microscopy (AFM) data (Fig. 1d, e). Mass-per-length (MPL) data (Supplementary Fig. 10) show a broad maximum centered at 40.1 kDa/nm, which corresponds to ~6 peptides, suggesting that three dimers associate in the mature fibril as the predominant structure under the experimental conditions used for scanning transmission electron microscopy (STEM). The ~10 nm length of each strand and the ~6 nm thickness of three associated dimers are also consistent with the fibril widths of 6–10 nm observed in negative-stain TEM images (Fig. 1c).

Discussion

The low-pH glucagon fibril structure we describe here is unique among amyloid fibril structures known to date by having two molecular conformations integrated within a single ultrastructural fibril morphology[39], thermodynamically favored antiparallel hydrogen bonding, and involvement of the full-length peptide in hydrogen bonding. The latter makes the glucagon β-strand the longest known among all peptides and proteins. In comparison, most neurodegenerative amyloid fibrils consist of parallel-in-register cross-β structures with one predominant molecular conformation and with significant numbers of disordered residues outside the β-sheet core[13,16,20,40,41]. The molecular conformational polymorphism of glucagon represents a new structural principle of amyloid assembly, and may be present in other amyloid fibrils as more atomic-resolution structures become available.

Due to the involvement of the entire peptide in cross-β hydrogen bonding, the glucagon fibril has a relatively uniform width of ~10 nm. The sidechain interfaces for the three dimers are also highly uniform, consistent with X-ray fiber diffraction data showing unusual periodicity in the equatorial plane[7]. The extraordinary length of the β-strand suggests that the peptide may zip up into fibrils from the two ends, promoted by favorable aromatic, hydrophobic and polar interactions along the way. Indeed, alanine scanning mutagenesis showed that fibrillization is slowed 3–10 fold by mutations at F6, V23 or M27, indicating the importance of the intermolecular interactions at these residues[42].

Glucagon is intrinsically disordered at low physiological concentrations (Fig. 4e)[43,44] before binding to its G-protein coupled receptor and acquiring an α-helical structure (Fig. 4g)[45]. At moderately higher concentrations glucagon forms α-helical trimers[46] (Fig. 4f), which are likely the species responsible for initiating fibril growth[47,48]. What is the cause of

glucagon's ability to convert among these multiple conformations, especially into a stable fibril with an unprecedented β-strand length? The structure of the fibril suggests that this conformational plasticity may result from the balance and complementarity between many types of residues: the peptide contains eleven polar residues (Ser, Thr, Gln, and Asn), three acidic Asp residues, four basic residues (His, Lys and Arg), five aromatic residues (Phe, Trp and Tyr) and five hydrophobic (Ala, Leu, Met and Val) residues. The equally spaced D9, D15 and D21 are neutralized at pH 2, thus promoting steric-zipper formation in conformer I (Fig. 4c), whereas at physiological pH, the anionic D9 and D15 are stabilized by cationic Arg residues in the receptor[45]. F6 and W25 form essential interactions with Y145 of helix I and W36 of extracellular loop 1 of the receptor, respectively, but are also ideally positioned to interact with each other to form the aromatic box in its fibrillar structure (Fig. 4d). Thus, the glucagon sequence encodes the ability to form a diverse set of three-dimensional structures. This is also manifested by the fact that glucagon can produce different fibril morphologies under different concentrations, pH, temperature and mechanical conditions[10,11]. At the pharmaceutical concentration of ~1 mg/ml, in addition to the straight fibrils studied here, a twisted fibril morphology also exists[49], and becomes dominant below 0.25 mg/ml. The fibril structure determined here is the more important form because its disruption should allow even higher concentrations of the peptide to be formulated in solution for potential applications in dual insulin/glucagon pumps.

Determination of the low-pH glucagon fibril structure opens the path for the rational design of glucagon analogs that resist fibril formation and increase the therapeutic efficacy. For example, previous mutagenesis studies found the F6A mutation to increase the lag time of fibril formation seven-fold[42]. The current structure suggests that this inhibition is due to the destabilizing effect of removing the aromatic interaction between F6 and W25. The activity-retaining mutation of Q3 to acetylated 2,4-diaminobutryic acid increased the solution stability[50], likely because of the disruption of the favorable polar interactions between Q3 and N28. Future studies should aim to identify mutations that not only destabilize the dimer-of-dimer β-sheet structure but also prevent adoption of alternative fibril structures, while at the same time retaining the receptor-binding activity of the native peptide in order to treat hypoglycemia.

Online Methods

Preparation of isotopically labeled glucagon fibrils

All peptides were purchased from Biopeptek Pharmaceuticals (Malvern, PA) and are >95% pure based on HPLC. Lyophilized peptide was dissolved in deionized water that was adjusted to pH 2 with HCl to produce a 13 mg/mL stock solution. The solution was briefly vortexed and when cloudy was subjected to bath sonication for less than a minute. The stock solution was filtered through a 0.2 μm syringe filter; the exact concentration after filtration was measured by UV spectroscopy at 280 nm using a molar extinction coefficient of 8250 M^{-1} cm^{-1}. This filtered stock solution was diluted to a final peptide concentration of 8 mg/mL and was incubated without shaking in eppendorf tubes for 7 days at 21°C. Solutions of ^{13}C, ^{15}N-labeled peptide were fibrillized after seeding with a 30–45 μl aliquot from a previously formed unlabeled glucagon fibril to a final "seed" concentration of 5% (600–900 μl).

Negative-stain transmission electron microscopy (TEM)

Negative-stain TEM images of the pH 2 glucagon fibrils were measured using an FEI Tecnai Spirit Bio-Twin Transmission Electron Microscope with an acceleration voltage of 120 kV. A 5 μl aliquot of the fibril solution was diluted 40-fold with water and mixed thoroughly. 5 μL of this diluted solution was deposited onto the surface of a 200 mesh carbon-coated copper grid (Electron Microscopy Sciences, Hatfield, PA). After 1 minute, excess liquid was blotted off using filter paper and the grid was rinsed briefly with 5 μL water. The rinse water was wicked away with filter paper and 5 μL 1% uranyl acetate was added to the grid as a negative stain to enhance contrast. After 1 minute, excess stain was blotted off and the grid was imaged immediately. Fibril width measurements were carried out using the program ImageJ.

Atomic force microscopy (AFM)

AFM images were obtained using a Cypher ES AFM (Asylum Research, Santa Barbara, CA) operating in alternate contact (tapping) mode with gold-coated ArrowUHF cantilevers. The cantilevers were driven at free air resonance (~1.2 MHz) via blueDrive™ photothermal excitation with the amplitude set point optimized to maintain net repulsive tip-sample interactions during the scan. A fibril stock solution (8 mg/ml) of 1–5 μL was deposited onto freshly cleaved mica (Ted Pella, Inc.), blotted with filter paper after ~30 s of incubation and allowed to air-dry before imaging. Samples were scanned at 512×512 pixel resolution at 4.88 Hz in air at ambient temperature. A first-order XY plane fit was applied to the images to remove sample tilt.

Circular dichroism (CD)

The secondary structure content of glucagon was analyzed using a JASCO J-1500 CD spectrophotometer using a 0.1 mm quartz cell. Ellipticity was measured on the pH 2 8 mg/mL peptide solution between 200 and 260 nm every hour for the first 24 hours, followed by discrete time points at day 3 and day 7. The raw data was converted to mean residue ellipticity using the equation $[\theta] = \theta_{obs}/10(l\,c\,r)$, where θ_{obs} is the measured ellipticity (mdeg), l is the path length (0.1 mm), c is the peptide concentration (M) and r is the number of residues in the peptide (29 for glucagon).

Dynamic light scattering (DLS)

DLS measurements were conducted on a Zetasizer Nano ZS instrument (Malvern Panalytical) using a reduced-volume plastic cuvette. An 8 mg/mL peptide solution at pH 2 was prepared as above. At time points of 0, 1, 3 and 7 days, 100 μL of the solution was transferred to the cuvette and measured with an acquisition time of 10 seconds. The number of acquisitions per measurement (~15) was determined by the instrument and not manually controlled. Representative autocorrelation functions of the scattered light intensities were plotted and normalized in GraphPad Prism to show particle size and polydispersity trends.

Mass-per-length (MPL) measurement by scanning transmission electron microscopy (STEM)

To determine the number of cross-β sheets in the fibril, we measured the MPL using STEM. Images were collected using an FEI TALOS microscope equipped with a field emission gun operating with an extraction voltage of 4.5 kV and an acceleration voltage of 200 kV. Microtubules formed by porcine brain tubulin (Cytoskeleton, Inc.) were used as a standard to calibrate the mass density in the images[51]. Tubulin is composed of a heterodimer of 55 kDa proteins[52]; each micron of microtubule contains 1650 heterodimers, thus giving an MPL of $55 \times 2 \times 1650/1000 = 181.5$ kDa/nm.

Microtubule solution was prepared following the protocol provided by Cytoskeleton, Inc. A tubulin buffer was prepared by resuspending lyophilized tubulin buffer powder in deionized water to give a pH 7 solution (16 mM PIPES, 0.4 mM $MgCl_2$, 0.1 mM EGTA). Then 99.1% pure lyophilized paclitaxel powder, which stabilizes microtubules, was resuspended in anhydrous dimethyl sulfoxide to give a 2 mM stock solution. About 100 μL of the paclitaxel solution was mixed with 10 mL of tubulin buffer, giving a resuspension buffer that was added to lyophilized microtubule powder containing 95% tubulin to a final concentration of 1 mg/mL.

Carbon-coated 200 mesh copper grids (CF200-Cu, Electron Microscopy Sciences, Inc.) were glow-discharged using a plasma cleaner (PDC-32G, Harrica Plasma, Inc.). About 4 μL of the microtubule solution was applied onto the grid, allowed to adsorb for 1 min, then blotted off. The grid was washed once with ~4 μL deionized water, blotted immediately, and dried for 5 min. To stain the microtubules (Supplementary Fig. 10a), 4 μl of a 1% phosphotungstic acid solution (pH 7) was applied to the grid, allowed to absorb for 30 s, then blotted off. These stained samples were examined in the bright field mode to verify the presence of the microtubules.

To measure the MPL of glucagon fibrils, 3 μl of glucagon fibril solution (8 mg/ml) was applied onto the grid that contains unstained microtubules, incubated for 30 s, blotted off and washed with deionized water three times. The grids were first imaged in bright field mode to find areas that contain both microtubules and glucagon. Then the specimens were adjusted to the eucentric height and the images were corrected for any astigmatism. The microscope was then switched to STEM mode and dark-field images were collected using a high-angle annular dark field (HAADF) detector with a camera length of 200 mm, a 2048×2048 image size, a single-pixel dwell time of 4 μs and a single-frame dwell time of 19.9 s. Only fibrils that are single and not laterally associated were imaged. The intensities of the dark-field STEM images were analyzed using ImageJ. The intensity of a selected area contains contributions from three sources: the proteins of interest, the carbon film of the grid and residual salts from the tubulin buffer. We subtracted the background salt and carbon film intensities from the protein intensities by selecting same-sized rectangles that contain proteins or that are empty. For the microtubules, we drew rectangles with a length of a along the long axis and with a width that encompasses the whole protein and recorded the integrated intensities I_{std}. We also recorded the background intensity I_{bkg1} in a same-size rectangle in a neighboring area without protein. For glucagon fibrils, rectangles with a length b were drawn over single fibrils and the integrated intensities I_{fibril} were recorded.

Intensities in an identical-sized rectangle in a neighboring empty area were recorded as I_{bkg2}. The MPL (kDa/nm) of glucagon was calculated as $MPL = (I_{fibril} - I_{bkg2}) \times (181.5 \ a)/.(I_{std} - I_{bkg1}) \ b$. About 290 data points were collected to obtain a statistically significant histogram of the glucagon fibril MPL.

Solid-state NMR experiments and data analysis

Glucagon fibrils in 500 μl of pH 2 solution at a concentration of 8 mg/ml were centrifuged at 40,000 rpm for 14 hours at 4°C directly into 3.2 mm magic-angle-spinning (MAS) rotors. 250 μl of supernatant was removed and another 250 μl of fibril suspension was added and centrifuged again. Typically, ~5 mg of peptide and 25–40 μl solvent were packed into each MAS rotor.

Most SSNMR experiments were conducted on a Bruker Avance II 800 MHz (18.8 T) spectrometer equipped with a 3.2 mm MAS probe tuned to ^{1}H, ^{13}C and ^{15}N frequencies (Supplementary Table 3). Additional spectra were measured on Avance III HD 600 MHz (14.1 T) and Avance 900 MHz (21.1 T) spectrometers. Samples were spun at MAS frequencies from 10.00 kHz to 15.75 kHz. Typical radiofrequency (rf) field strengths were 50–71 kHz for ^{1}H, 50 kHz for ^{13}C and 35–39 kHz for ^{15}N. ^{13}C chemical shifts were externally referenced to the 38.48 ppm adamantane CH_2 peak on the TMS scale. ^{15}N chemical shifts were externally referenced to the 122.00 ppm N-acetylvaline amide peak on the liquid ammonia scale. Most spectra were measured between 268 K and 293 K, as reported by the probe thermocouple. At MAS frequencies of 10.00–15.75 kHz, frictional heating makes the sample temperatures 5–10 K warmer than the thermocouple-reported values[53]. The NMR spectra were processed using TopSpin and assigned in Sparky[54].

2D ^{13}C-^{13}C correlation spectra for ^{13}C chemical shift assignment and for identifying long-range spatial contacts were measured using Dipolar-Assisted Rotational Resonance (DARR)[55] and COmbined $R2_n{}^\nu$-Driven (CORD)[56] experiments. For resonance assignment, the DARR and CORD mixing times were 50 and 30 ms, respectively. For water-edited 2D ^{13}C-^{13}C correlation experiments, a ^{1}H T_2 filter of 1.4–1.7 ms and a 2.25 ms ^{1}H-^{1}H spin diffusion period was inserted before ^{1}H-^{13}C cross polarization (CP), in order to transfer the water ^{1}H magnetization to the peptide protons[28,32].

To identify inter-residue correlations that constrain the three-dimensional packing of the peptide, we measured three types of 2D ^{13}C-^{13}C correlation spectra. The first type of experiments was Proton-Driven Spin-diffusion (PDSD) with mixing times of 0.5 or 1.0 s or CORD mixing for 250 or 500 ms. The second experiment was proton-assisted recoupling (PAR)[23] with a mixing time of 12 ms and ^{1}H and ^{13}C rf fields of 50 and 53 kHz, respectively. The third experiment was CHHC[27], which began with a 700 μs ^{1}H-^{13}C CP and ^{13}C t_1 evolution, followed by reverse transfer of ^{13}C magnetization to the directly bonded protons with a 75 μs CP period. This was followed by a 200 μs ^{1}H-^{1}H spin diffusion period, after which another 75 μs ^{1}H-^{13}C CP transferred the magnetization to ^{13}C for detection.

^{15}N chemical shifts were measured using the ^{15}N-^{13}C Transferred-Echo Double Resonance (TEDOR)[57,58] experiment and the SPECtrally Induced Filtering In Combination with Cross Polarization (^{SPECIFIC}CP)[59] experiment. The TEDOR period was 1.2–1.4 ms while the

SPECIFICCP period was 3.5 ms. Before ^{13}C detection, a 79–150 ms ^{13}C-^{13}C spin diffusion was used to correlate ^{15}N chemical shifts with sidechain ^{13}C chemical shifts.

The absolute chemical shift difference $|\delta C(I) - \delta C(II)|$ between conformers I and II for each residue was calculated as $\left[\sum_{C_i} \left(\delta^I_{C_i} - \delta^{II}_{C_i} \right)^2 / n \right]^{1/2}$, where *n is* 2 for Gly and 3 for all other residues.

Backbone (ϕ, ψ) torsion angles were predicted from the measured ^{13}C and ^{15}N chemical shifts using the TALOS-N software[60], which takes ^{13}Cα, ^{13}Cβ, ^{13}CO and ^{15}N chemical shifts and the amino acid sequence and compares them with a database of protein chemical shifts and torsion angles to determine the secondary structure of the peptide.

Structure calculation

The glucagon fibril structure was calculated using CYANA 2.1[61]. Structure calculations included two β-sheets of 8 monomers each. Monomers were connected using LL5 linkers, which behave as pseudo-atoms that do not affect the calculated target function. Conformers I and II alternate in the 8 planes perpendicular to the fibril axis. Within each plane, homodimer C_2 symmetry was enforced by the inclusion of torsion angle and relative Cα position symmetry terms in the CYANA target function (weight_ide = 1.0 and weight_sym = 0.1, respectively). To maintain the homodimer C_2 symmetry, we set conformer I-II intermolecular contacts for molecule pairs in which the odd-numbered residues of conformer I are the backbone hydrogen-bond donors and odd-numbered residues of conformer II are the hydrogen-bond acceptor. Structure calculation runs with switched I-II pairs resulted in the same target function and RMSD as the structure presented herein. To keep inter-layer distances consistent with the known cross-β inter-sheet distances of 4.8 Å[62], the backbones between every other layer of the same conformer were constrained between 9.3 and 9.9 Å; these constraints were given a ten-fold greater weight than others. The parallel homomeric interface within each layer comprises even-numbered residues, S2–N28, for conformer I and odd-numbered residues, Q3–M27, for conformer II. This homomeric interface was constrained by an upper distance limit of 10.0 Å between Cα atoms of the same residue, in order to be consistent with the known inter-sheet distance of ~10 Å for amyloid fibril steric zippers. Chemical-shift derived (ϕ, ψ) angles were applied as torsion angle restraints for both conformers I and II; the range was set to be twice the uncertainty given by TALOS-N. For residues S2–T29, which had chemical shifts characteristic of a β-sheet conformation, we imposed hydrogen bonds by setting the O-H^N distances to 1.5–1.7 Å and the O-N distances to 2.5–2.7 Å. These constraints were given a ten-fold greater weight than others. Upper distance limits for cross peaks observed in various 2D spectra (Supplementary Data Set 2) were set as 6 Å for 200 µs CHHC spectra and spectra with ^{13}C spin diffusion mixing times shorter than 100 ms; 7 Å for 250 ms spin diffusion spectra; 8 Å for 500 ms and 1.0 s spin diffusion spectra on an 800 MHz spectrometer and for the 15 ms PERSPIRATIONCP spectra[24], 8.5 Å for 500 ms spin diffusion spectra on a 600 MHz spectrometer, and 9 Å for the 12 ms PAR spectra. Upper distance limits were increased by 1.5 Å for Trp sidechains to account for relayed transfers across the rigid, bulky indole rings. 700 individual trajectories were run

with 150,000 torsion angle steps each. The ten structures with the lowest CYANA target function were included in the final ensemble.

Supplementary Material

Refer to Web version on PubMed Central for supplementary material.

Acknowledgements

References

1. Chiti F & Dobson CM Protein Misfolding, Amyloid Formation, and Human Disease: A Summary of Progress Over the Last Decade. Annu. Rev. Biochem 86, 27–68 (2017). [PubMed: 28498720]

2. Frokjaer S & Otzen DE Protein drug stability: a formulation challenge. Nat. Rev. Drug Discov 4, 298 (2005). [PubMed: 15803194]

3. Brange J, Andersen L, Laursen ED, Meyn G & Rasmussen E Toward understanding insulin fibrillation. J. Pharm. Sci 86, 517–525 (1997). [PubMed: 9145374]

4. Habegger KM et al. The metabolic actions of glucagon revisited. Nat. Rev. Endocrinol 6, 689 (2010). [PubMed: 20957001]

5. Caputo N et al. Mechanisms of glucagon degradation at alkaline pH. Peptides 45, 40–47 (2013). [PubMed: 23651991]

6. Beaven GH, Gratzer WB & Davies HG Formation and structure of gels and fibrils from glucagon. Eur. J. Biochem 11, 37–42 (1969). [PubMed: 5353602]

7. Andersen CB et al. Glucagon fibril polymorphism reflects differences in protofilament backbone structure. J. Mol. Biol 397, 932–46 (2010). [PubMed: 20156459]

8. Oliveira CL et al. A SAXS study of glucagon fibrillation. J. Mol. Biol 387, 147–161 (2009). [PubMed: 19385046]

9. Dong M et al. AFM-based force spectroscopy measurements of mature amyloid fibrils of the peptide glucagon. Nanotechnology 19, 384013 (2008). [PubMed: 21832572]

10. Pedersen JS et al. The changing face of glucagon fibrillation: structural polymorphism and conformational imprinting. J. Mol. Biol 355, 501–23 (2006). [PubMed: 16321400]

11. De Jong KL, Incledon B, Yip CM & DeFelippis MR Amyloid fibrils of glucagon characterized by high-resolution atomic force microscopy. Biophys. J 91, 1905–14 (2006). [PubMed: 16766610]

12. Gratzer WB, Bailey E & Beaven GH Conformational states of glucagon. Biochem. Biophys. Res. Commun 28, 914–919 (1967). [PubMed: 6064594]

13. Colvin MT et al. Atomic resolution structure of monomorphic $A\beta_{42}$ amyloid fibrils. J. Am. Chem. Soc 138, 9663–9674 (2016). [PubMed: 27355699]

14. Wälti MA et al. Atomic-resolution structure of a disease-relevant Aβ(1–42) amyloid fibril. Proc. Natl. Acad. Sci. U. S. A 113, E4976–E4984 (2016). [PubMed: 27469165]

15. Tuttle MD et al. Solid-state NMR structure of a pathogenic fibril of full-length human α-synuclein. Nat. Struct. Mol. Biol 23, 409 (2016). [PubMed: 27018801]

16. Fitzpatrick AWP et al. Cryo-EM structures of tau filaments from Alzheimer's disease. Nature 547, 185 (2017). [PubMed: 28678775]

17. Sawaya MR et al. Atomic structures of amyloid cross-beta spines reveal varied steric zippers. Nature 447, 453–457 (2007). [PubMed: 17468747]

18. Antzutkin ON et al. Multiple quantum solid-state NMR indicates a parallel, not antiparallel, organization of β-sheets in Alzheimer's β-amyloid fibrils. Proc. Natl. Acad. Sci 97, 13045–13050 (2000). [PubMed: 11069287]

19. Paravastu AK, Leapman RD, Yau W-M & Tycko R Molecular structural basis for polymorphism in Alzheimer's β-amyloid fibrils. Proc. Natl. Acad. Sci. U. S. A 105, 18349–18354 (2008). [PubMed: 19015532]

20. Petkova AT, Yau W-M & Tycko R Experimental constraints on quaternary structure in alzheimer's β-amyloid fibrils. Biochemistry 45, 498–512 (2006). [PubMed: 16401079]

21. Tycko R Amyloid polymorphism: structural basis and neurobiological relevance. Neuron 86, 632–45 (2015). [PubMed: 25950632]

22. Hiller S et al. Solution structure of the integral human membrane protein VDAC-1 in detergent micelles. Science 321, 1206–1210 (2008). [PubMed: 18755977]

23. Paëpe GD, Lewandowski JR, Loquet A, Böckmann A & Griffin RG Proton assisted recoupling and protein structure determination. J. Chem. Phys 129, 245101 (2008). [PubMed: 19123534]

24. Gelenter MD & Hong M Efficient ^{15}N–^{13}C polarization transfer by third-spin-assisted pulsed cross-polarization magic-angle-spinning NMR for protein structure determination. J. Phys. Chem. B 122, 8367–8379 (2018). [PubMed: 30106585]

25. Wasmer C et al. Amyloid fibrils of the HET-s(218–289) prion form a beta solenoid with a triangular hydrophobic core. Science 319, 1523–1526 (2008). [PubMed: 18339938]

26. Qiang W, Yau W-M, Luo Y, Mattson MP & Tycko R Antiparallel β-sheet architecture in Iowa-mutant β-amyloid fibrils. Proc. Natl. Acad. Sci. U. S. A 109, 4443–4448 (2012). [PubMed: 22403062]

27. Lange A, Luca S & Baldus M Structural constraints from proton-mediated rare-spin correlation spectroscopy in rotating solids. J. Am. Chem. Soc 124, 9704–9705 (2002). [PubMed: 12175218]

28. Wang T, Jo H, DeGrado WF & Hong M Water Distribution, Dynamics, and Interactions with Alzheimer's β-Amyloid Fibrils Investigated by Solid-State NMR. J. Am. Chem. Soc 139, 6242–6252 (2017). [PubMed: 28406028]

29. Mandala VS, Gelenter MD & Hong M Transport-relevant protein conformational dynamics and water dynamics on multiple time scales in an archetypal proton channel: Insights from solid-state NMR. J. Am. Chem. Soc 140, 1514–1524 (2018). [PubMed: 29303574]

30. Lesage A & Bockmann A Water-protein interactions in microcrystalline Crh measured by H-1-C-13 solid-state NMR spectroscopy. J. Am. Chem. Soc 125, 13336–13337 (2003). [PubMed: 14583011]

31. Liepinsh E & Otting G Proton exchange rates from amino acid side chains— implications for image contrast. Magn. Reson. Med 35, 30–42 (1996). [PubMed: 8771020]

32. Williams JK & Hong M Probing membrane protein structure using water polarization transfer solid-state NMR. J. Magn. Reson 247, 118–127 (2014). [PubMed: 25228502]

33. Gallivan JP & Dougherty DA Cation-pi interactions in structural biology. Proc. Natl. Acad. Sci. U. S. A 96, 9459–9464 (1999). [PubMed: 10449714]

34. Serrano L, Bycroft M & Fersht AR Aromatic-aromatic interactions and protein stability. Investigation by double-mutant cycles. J. Mol. Biol 218, 465–475 (1991). [PubMed: 2010920]

35. Meyer EA, Castellano RK & Diederich F Interactions with aromatic rings in chemical and biological recognition. Angew. Chem. Int. Ed. Engl 42, 1210–1250 (2003). [PubMed: 12645054]

36. Choma C, Gratkowski H, Lear JD & DeGrado WF Asparagine-mediated self-association of a model transmembrane helix. Nat. Struc. Biol 7, 161–166 (2000).

37. Lear JD, Gratkowski H, Adamian L, Liang J & DeGrado WF Position-dependence of stabilizing polar interactions of asparagine in transmembrane helical bundles. Biochemistry 42, 6400–7 (2003). [PubMed: 12767221]

38. Deechongkit S et al. Context-dependent contributions of backbone hydrogen bonding to beta-sheet folding energetics. Nature 430, 101–105 (2004). [PubMed: 15229605]

39. Elkins MR et al. Structural polymorphism of alzheimer's β-Amyloid fibrils as controlled by an E22 switch: a solid-state NMR study. J. Am. Chem. Soc 138, 9840–9852 (2016). [PubMed: 27414264]

40. Helmus JJ, Surewicz K, Nadaud PS, Surewicz WK & Jaroniec CP Molecular conformation and dynamics of the Y145Stop variant of human prion protein in amyloid fibrils. Proc. Natl. Acad. Sci. U. S. A 105, 6284–6289 (2008). [PubMed: 18436646]

41. Mompeán M et al. The Structure of the Necrosome RIPK1-RIPK3 Core, a Human Hetero-Amyloid Signaling Complex. Cell 173, 1244–1253 (2018). [PubMed: 29681455]

42. Pedersen JS, Dikov D & Otzen DE N- and C-terminal hydrophobic patches are involved in fibrillation of glucagon. Biochemistry 45, 14503–12 (2006). [PubMed: 17128989]

43. Boesch C, Bundi A, Oppliger M & Wüthrich K ^{1}H nuclear-magnetic-resonance studies of the molecular conformation of monomeric glucagon in aqueous solution. Eur. J. Biochem 91, 209–214 (1978). [PubMed: 720338]

44. Braun W, Wider G, Lee KH & Wüthrich K Conformation of glucagon in a lipid-water interphase by ^{1}H nuclear magnetic resonance. J. Mol. Biol 169, 921–948 (1983). [PubMed: 6631957]

45. Zhang H et al. Structure of the glucagon receptor in complex with a glucagon analogue. Nature 553, 106–110 (2018). [PubMed: 29300013]

46. Sasaki K, Dockerill S, Adamiak DA, Tickle IJ & Blundell T X-ray analysis of glucagon and its relationship to receptor binding. Nature 257, 751–757 (1975). [PubMed: 171582]

47. Svane AS et al. Early stages of amyloid fibril formation studied by liquid-state NMR: the peptide hormone glucagon. Biophys. J 95, 366–77 (2008). [PubMed: 18339765]

48. Moorthy BS, Ghomi HT, Lill MA & Topp EM Structural transitions and interactions in the early stages of human glucagon amyloid fibrillation. Biophys. J 108, 937–48 (2015). [PubMed: 25692598]

49. Andersen CB, Otzen D, Christiansen G & Rischel C Glucagon amyloid-like fibril morphology is selected via morphology-dependent growth inhibition. Biochemistry 46, 7314–24 (2007). [PubMed: 17523599]

50. Chabenne J et al. A glucagon analog chemically stabilized for immediate treatment of life-threatening hypoglycemia. Mol. Metab 3, 293–300 (2014). [PubMed: 24749059]

51. Tian Y et al. Nanotubes, Plates, and Needles: Pathway-Dependent Self-Assembly of Computationally Designed Peptides. Biomacromolecules, Epub ahead of print (2018).

52. Amos LA & Klug A Arrangement of subunits in flagellar microtubules. J. Cell Sci 14, 523–549 (1974). [PubMed: 4830832]

53. Bernard GM et al. Methylammonium lead chloride: A sensitive sample for an accurate NMR thermometer. J. Magn. Reson 283, 14–21 (2017). [PubMed: 28843057]

54. Lee W, Tonelli M & Markley JL NMRFAM-SPARKY: enhanced software for biomolecular NMR spectroscopy. Bioinformatics 31, 1325–1327 (2015). [PubMed: 25505092]

55. Takegoshi K, Nakamura S & Terao T ^{13}C–^{1}H dipolar-assisted rotational resonance in magic-angle spinning NMR. Chem. Phys. Lett 344, 631–637 (2001).

56. Hou G, Yan S, Trébosc J, Amoureux J-P & Polenova T Broadband homonuclear correlation spectroscopy driven by combined R2^{nv} sequences under fast magic angle spinning for NMR structural analysis of organic and biological solids. J. Magn. Reson 232, 18–30 (2013). [PubMed: 23685715]

57. Hing AW, Vega S & Schaefer J Transferred-echo double-resonance NMR. J. Magn. Reson 96, 205–209 (1992).

58. Daviso E, Eddy MT, Andreas LB, Griffin RG & Herzfeld J Efficient resonance assignment of proteins in MAS NMR by simultaneous intra- and inter-residue 3D correlation spectroscopy. J. Biomol. NMR 55, 257–265 (2013). [PubMed: 23334347]

59. Baldus M, Petkova AT, Herzfeld J & Griffin RG Cross polarization in the tilted frame: assignment and spectral simplification in heteronuclear spin systems. Mol. Phys 95, 1197–1207 (1998).

60. Shen Y & Bax A Protein backbone and sidechain torsion angles predicted from NMR chemical shifts using artificial neural networks. J. Biomol. NMR 56, 227–241 (2013). [PubMed: 23728592]

61. Güntert P, Mumenthaler C & Wüthrich K Torsion angle dynamics for NMR structure calculation with the new program DYANA. J. Mol. Biol 273, 283–298 (1997). [PubMed: 9367762]

62. Jeppesen MD, Hein K, Nissen P, Westh P & Otzen DE A thermodynamic analysis of fibrillar polymorphism. Biophys. Chem 149, 40–6 (2010). [PubMed: 20435401]
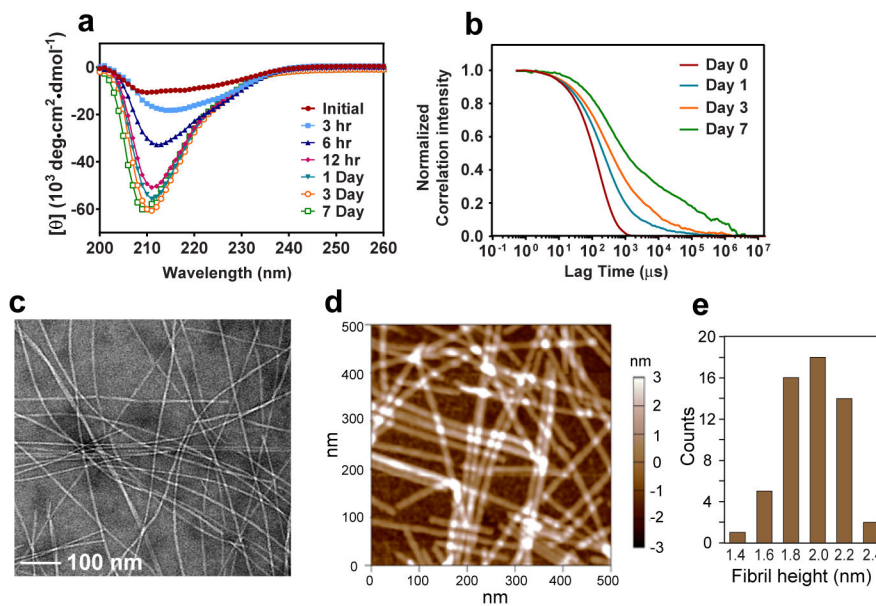
Figure 1.
Glucagon forms well-ordered amyloid fibrils at acidic pH. **a**, Circular dichroism spectra of 8 mg/mL glucagon solution over 7 days. Predominantly β-strand spectra are observed within 12 hours. **b**, Autocorrelation functions of scattered light intensities show slower and more disperse decays over time, indicating an increase in the average particle sizes and the polydispersity of particle sizes. **c**, Representative negative-stain TEM image of glucagon fibrils, showing predominantly straight fibrils with occasional twists. **d**, AFM image of the glucagon fibrils, showing an average height of 1.97±0.22 nm (mean and s.d. of n = 56 measurements of fibrils), consistent with a dimer unit in the cross section normal to the fibril axis. **e**, Histogram of fibril height statistics from the AFM image, showing a peak at ~2 nm.

Figure 2.
Glucagon fibrils contain two distinct β-strand conformations. **a**, Representative 2D ^{13}C-^{13}C correlation spectrum with 30 ms ^{13}C spin diffusion (SD), showing well resolved chemical shifts of the glucagon fibrils. **b**, Representative 2D ^{15}N-$^{13}C\alpha$ correlation spectrum. **c**, Selected 2D ^{13}C-^{13}C and ^{15}N-^{13}C spectra reveal peak doubling, indicating the coexistence of two molecular conformations. **d**, Strips of 3D NCACX (black) and NCOCX (green) correlation spectra, illustrating sequential resonance assignment. **e**, Absolute chemical shift differences between conformers I and II. Purple bars above the diagram indicate segments for which conformers I and II are unambiguously assigned from the sequential cross peaks, whereas black lines indicate connectivities between residues that are far away in the amino acid sequence, which help to distinguish conformer I and conformer II. **f**, Backbone (ϕ, ψ) torsion angles obtained from the experimental ^{13}C and ^{15}N chemical shifts. Both conformers correspond to a continuous β-strand.

Figure 3.
2D NMR spectra indicate that glucagon forms antiparallel β-sheets with two distinct steric zipper interfaces. **a**, 500 ms ^{13}C SD spectra of sample 3 without or with dilution. M27-T5 and M27-F6 cross peaks are observed, whose intensities decrease significantly upon dilution of the labeled peptide with unlabeled peptide, supporting antiparallel packing of conformers I and II. **b**, 500 ms ^{13}C SD spectra of sample 9c. Y13-R18 correlations indicate cation-π interaction. **c**, 500 ms ^{13}C SD spectra of sample 2 show H1–T29 cross peaks, indicating that the two termini of the peptide come into close proximity. **d**, 200 μs CHHC spectrum of sample 1. Strong V23-S8 Cα-Cα cross peaks indicate that the antiparallel packing is along the hydrogen-bonded fibril axis. **e**, Summary of measured inter-residue correlations. Conformer I – I correlations are shown below the diagonal, whereas conformer II – II correlations are shown above the diagonal. These sequential contacts contain both intramolecular and intermolecular contributions and are shown as open squares. The unambiguously intermolecular conformer I – conformer II contacts are shown as black squares, with the x-axis indicating conformer I and the y-axis indicating conformer II. **f**, Full and water-edited 2D spectra of sample 8c. Residues T5, T7, and S11 are well hydrated in conformer II but dehydrated in conformer I, indicating that the water-accessible surfaces differ between the two conformers. **g**, Intensity ratios between the water-edited spectra and full spectra, showing relative water accessibility of the sidechains. Even-numbered residues are more hydrated (high S/S_0 values) in conformer I whereas odd-numbered residues are more hydrated in conformer II. **h**, Schematic of the glucagon β-strand packing. The fibrils

contain two distinct β-strands that hydrogen-bond in antiparallel along the fibril axis. The two strands in each homodimer cross section have C_2 symmetry around an axis parallel to the peptide backbone.
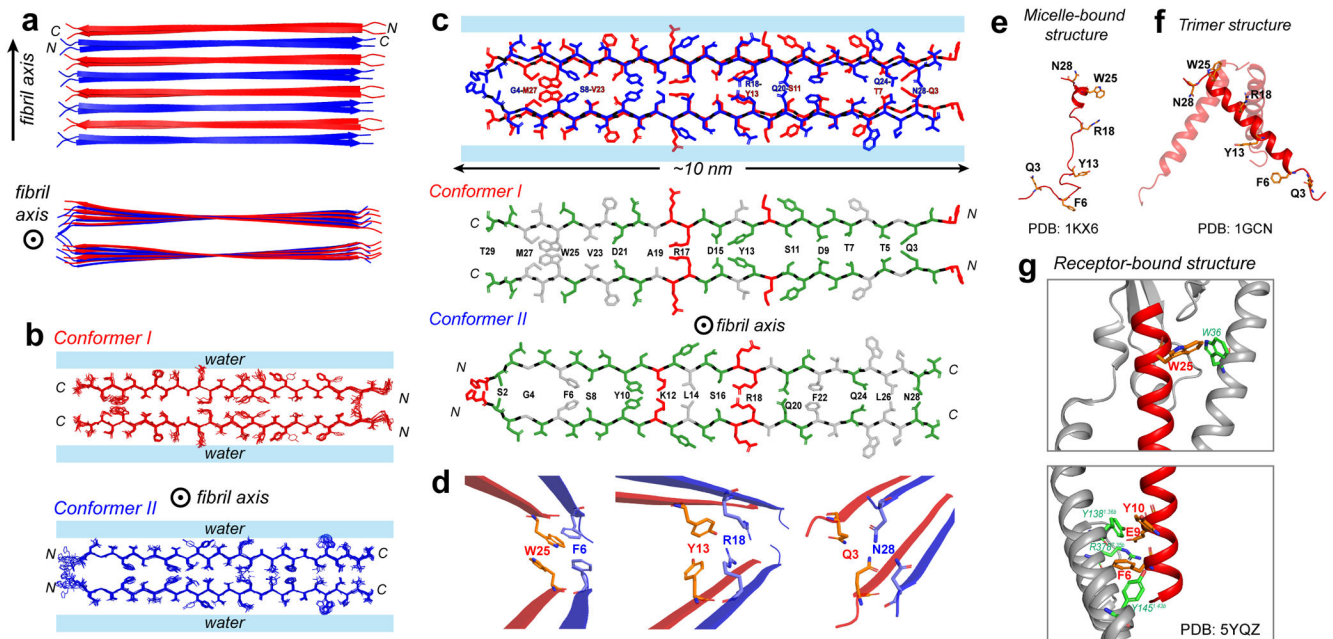
Figure 4.
Atomic structure of the low-pH glucagon fibril. **a**, Top and side view of the fibril. Conformer
I (red) and conformer II (blue) alternate and hydrogen-bond in antiparallel. Each conformer
forms a parallel homodimer as the basic repeat unit in the cross section normal to the fibril
axis. **b**, Ensemble of 10 lowest-energy structures viewed down the fibril axis. For clarity,
conformers I and II are shown separately. **c**, Sidechain packing in the dimer-of-dimer subunit
of glucagon fibrils. Each conformer self-associates in parallel, exhibiting C_2 symmetry in the
cross section normal to the fibril axis. Conformer I packs odd-numbered residues at the
steric zipper interface whereas conformer II packs even-numbered residues at the steric
zipper interface. Hydrophobic sidechains are colored white, polar residues are green and
positively charged residues are red. **d**, Zoomed-in views of F6–W25, Y13-R18 and Q3–N28
sidechain packing, which stabilize the fibril structure. This antiparallel fibril structure
contrasts with the glucagon structures in solution and as bound to its receptor. **e**, The
micelle-bound glucagon is mostly disordered (PDB 1KX6)[43,44]. **f**, The crystal structure of
glucagon (PDB 1GCN) is predominantly an α-helical trimer, which may be the precursor to
the β-sheet fibril. **g**, When bound to its G-protein coupled receptor in the lipid membrane,
glucagon is fully α-helical[45] (PDB5YQZ) and has many stabilizing interactions with the
receptor.

Table 1.

Glucagon peptides containing uniformly ^{13}C, ^{15}N-labeled residues (bold) used in this study.

Sample #	^{13}C, ^{15}N-labeled residues
1	HSQG**T** FT**S**DY SKY**LD** SRRA**Q** DF**V**QW LMNT
2	**H**SQGT FTSDY **S**KYLD SRRAQ DFVQW **L**MN**T**
3	H**S**QG**T F**TSDY SKYLD S**R**RAQ DFVQW L**M**NT
4	HS**Q**GT F**T**SD**Y** SKYLD S**R**RAQ D**F**VQW LMNT
7c	HS**QGT** FTSDY SKYLD SRRAQ DFV**QW LMN**T
8c	HSQG**T FTSDY S**KYLD SRRA**Q DFVQ**W LMNT
9c	HSQGT FTSDY **SKYLD SRRA**Q DFVQW LMNT
11	HSQGT FTSDY SKYLD SRRA**Q** DFVQW **LM**NT
12	HSQG**T** FTSDY **S**KYLD SRRAQ DFVQW LMNT

Table 2.

NMR and refinement statistics for the low-pH glucagon amyloid fibril.

	Glucagon fibril (PDB 6NZN)
NMR distance and dihedral constraints	
Distance constraints	
Total NOE	635×2
Inter-residue	635×2
Sequential ($|i-j| = 1$)	231×2
Medium range ($2 \le |i-j| \le 4$)	119×2
Long range ($|i-j| \ge 5$)	0
Intermolecular	285×2
Hydrogen bonds	27×2
Total dihedral-angle restraints	
ϕ	54×2
ψ	54×2
Structure statistics	
Violations (mean ± s.d.)	
Distance constraints (Å)	0.016 ± 0.001
Dihedral-angle constraints (°)	0.35 ± 0.03
Max. dihedral-angle violation (°)	3.9 ± 0.7
Max. distance-constraint violation (Å)	0.39 ± 0.06
Deviations from idealized geometry	
Bond lengths (Å)	0.00 ± 0.00
Bond angles (°)	0.49 ± 0.01
Impropers (°)	0.00 ± 0.00
Average pairwise r.m.s. deviation (Å)[a]	
Heavy	1.67
Backbone	0.80

[a]Pairwise r.m.s.d. was calculated among 10 refined structures.